GEOLOGY | THE GEOLOGICAL SOCIETY OF AMERICA®

https://doi.org/10.1130/G52548.1

Manuscript received 5 July 2024
Revised manuscript received 6 September 2024
Manuscript accepted 23 September 2024

Published online 9 October 2024

Sediment supply variation control on Lower Eocene delta sequences (Tremp Basin, Spain)

Romain Vaucher[1,2,*], Claire Musajo[2], Jorge E. Spangenberg[3], Miquel Poyatos-Moré[4], Christian Zeeden[5], Cai Puigdefàbregas[6], Marine Prieur[1], Sébastien Castelltort[1], and Thierry Adatte[2]

[1]Department of Earth Sciences, University of Geneva, Rue des Maraîchers 13, 1205 Geneva, Switzerland
[2]Institute of Earth Sciences (ISTE), University of Lausanne, Géopolis, 1015 Lausanne, Switzerland
[3]Institute of Earth Surface Dynamics (IDYST), Géopolis, University of Lausanne, 1015 Lausanne, Switzerland
[4]Departament de Geologia, Universitat Autònoma de Barcelona, 08193 Cerdanyola del Vallés, Spain
[5]Leibniz Institute for Applied Geophysics (LIAG), Geozentrum Hannover, 30655 Hannover, Germany
[6]Department of Earth and Ocean Dynamics, University of Barcelona, Carrer de Martí i Franquès, s/n, 08028 Barcelona, Spain

ABSTRACT

Sediment supply variations are often overlooked when interpreting depositional sequences, with most studies instead emphasizing changes in accommodation space. Here, we investigated a temporally well-constrained shallow-marine succession in the Tremp Basin to test the control of sediment supply variations on the development of deltaic sequences during the early Eocene. We analyzed the paleoenvironmental record (sedimentary facies and $\delta^{13}C_{org}$ values) of the Morillo Limestone and the Castigaleu Formation (52.2–50.6 Ma). The first progradation of the deltaic system is marked by the abrupt appearance of thick delta-front sandstones and associated with the first negative carbon isotopic excursions (CIEs) in the measured $\delta^{13}C_{org}$ record. Subsequent phases of progradation align with subsequent negative CIEs. Conversely, positive CIEs correspond to finer-grained, more-distal prodelta deposits. A series of hyperthermal events occurred during the deposition, globally identified as negative CIEs on $\delta^{13}C_{carb}$ reference curves, which we tentatively correlate with our $\delta^{13}C_{org}$ data. We therefore suggest that during deposition of this Lower Eocene shallow-marine succession, the primary trigger behind sequence generation was the high-frequency climate-induced variation in sediment supply, specifically the hyperthermal events, rather than changes in accommodation. This linkage underscores the complex interactions between climate dynamics and sedimentary responses that shape the stratigraphic architecture of shallow-marine settings.

INTRODUCTION

Accommodation (δA) and sediment supply (δS) variations can generate depositional sequences (Jervey, 1988; Schlager, 1993; Muto and Steel, 1997; Burgess and Prince, 2015; Zhang et al., 2019). δA is influenced by factors such as tectonic subsidence and uplift, eustatic sea-level fluctuations, and sediment compaction (Jervey, 1988), while δS encompasses factors like sediment transport processes, shifts in sediment sources, and climate conditions (Catuneanu et al., 2009). Although δA and δS are equally difficult to measure and analyze, δA is frequently emphasized as the dominant control on depositional sequences (Burgess, 2016). Disentangling the influences of δA and δS on the origin of stratigraphic sequences therefore poses significant challenges in interpretation, mainly due to the controlling factors having a nonunique resulting stratigraphic pattern (Burgess and Prince, 2015).

To assess the role of sediment supply in stratigraphic sequences, it is crucial to consider scenarios with limited eustatic variability, continuous subsidence, and highly variable sediment supply. Here, we analyzed paleoenvironmental variations recorded in a Lower Eocene shallow-marine succession deposited in the confined and continuously subsiding Tremp Basin, southern Pyrenees, Spain (Fig. 1). Deposition occurred during the early Eocene climatic optimum (EECO; 53.26–49.14 Ma), representing a hothouse climate with high atmospheric CO_2 concentrations, elevated temperatures, and ice-free poles (e.g., Westerhold et al., 2020). The EECO was also punctuated by several orbitally forced hyperthermal events lasting ~50–200 k.y., which involved abrupt and substantial releases of isotopically depleted carbon into the ocean-atmosphere system, identified globally in sedimentary records by distinctive negative carbon isotope excursions (CIEs) (Westerhold et al., 2020). By analogy with the Paleocene–Eocene thermal maximum (which lasted ~200 k.y.) and the middle Eocene climatic optimum (which lasted ~500 k.y.), which were short-lived warming events associated with progradation of coarse sediment and export of terrestrial clayey material (Foreman et al., 2012; Chen et al., 2018; Peris Cabré et al., 2023; Vimpere et al., 2023; Prieur et al., 2024), we hypothesized that similar sedimentary responses would be recorded during the multiple hyperthermal events of the EECO in the Tremp Basin.

GEOLOGIC SETTING

The Pyrenees (Fig. 1) formed as a result of the collision and subsequent subduction of the Iberian plate under the Eurasian plate (Ford et al., 2022). Orogeny occurred from the Late Cretaceous to early Miocene, developing south-directed thrust sheets and duplex structures, including the Axial Zone and the South Pyrenean Central Unit (SPCU) (Muñoz, 1992). The Bóixols, Montsec, and Serres Marginals are major SPCU thrusts, which detached in Triassic evaporite-rich strata (Puigdefàbregas and Souquet, 1986) to form the Mesozoic and Cenozoic Organyà, Tremp, and Àger piggyback basins (Muñoz et al., 2013). The Lower Eocene Morillo Limestone and Castigaleu Formation (Figs. 1A and 1B), deposited within the con-

Romain Vaucher https://orcid.org/0000-0003-3051-4128
*romain.vaucher88@gmail.com

CITATION: Vaucher, R., et al., 2025, Sediment supply variation control on Lower Eocene delta sequences (Tremp Basin, Spain): Geology, v. 53, p. 83–88, https://doi.org/10.1130/G52548.1

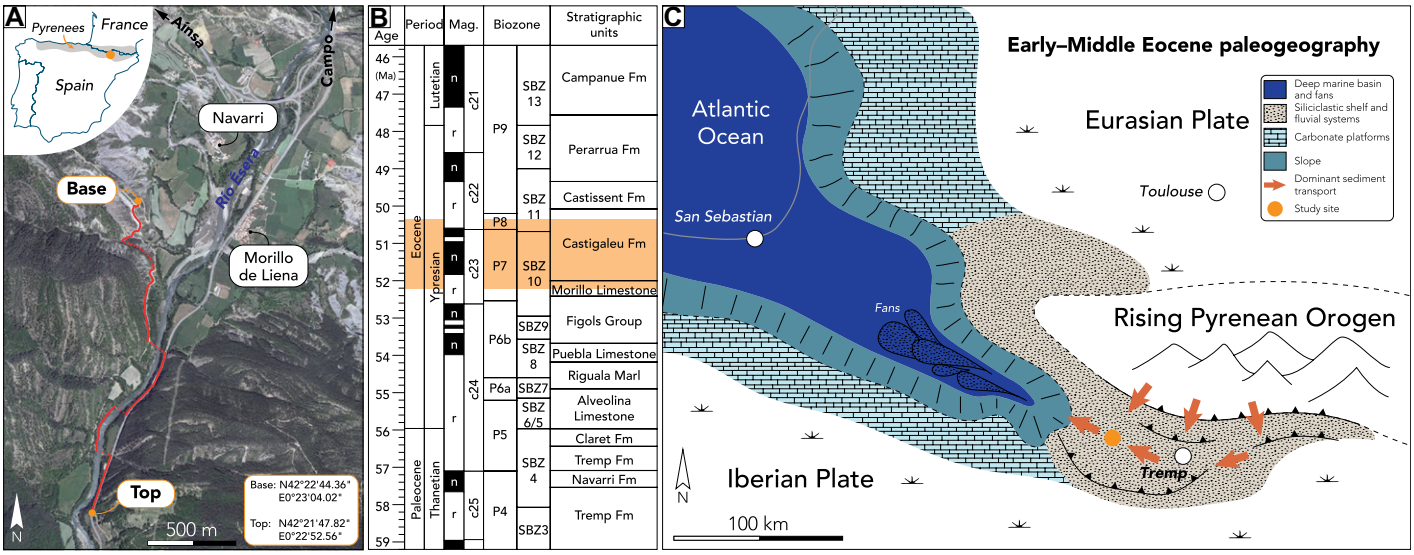

Figure 1. (A) Map of study area (Navarri, Spain). Red line indicates section logged along Río Ésera. (B) Paleocene–Eocene chronostratigraphic diagram of Tremp Basin (after Chanvry et al., 2018, and references therein). Studied interval is shown in orange; n—normal; r—reversed. (C) Simplified reconstruction of Pyrenean area during early–middle Eocene, modified after Castelltort et al. (2017).

fined and stratigraphically well-constrained Tremp Basin (Chanvry et al., 2018), were the focus of this study (Fig. 1C). The chronostratigraphic framework for the studied stratigraphic units was previously established via magnetobiostratigraphy (Bentham and Burbank, 1996).

METHODS

A 644-m-thick stratigraphic section along the Río Ésera near Navarri (Spain) was logged and sampled (Figs. 1–3). Stratal thicknesses were measured, and bed geometries, bounding contacts, grain size, sedimentary structures, and fossil contents were described (Figs. 2 and 3). Fresh rock samples were collected ($n = 293$) from sandstone and mudstone, cleaned, dried, and crushed. The organic carbon isotopic ratio ($\delta^{13}C_{org}$, ‰ relative to Vienna Peedee belemnite [VPDB]) was measured on decarbonated samples using an elemental analyzer (Carlo Erba 1108 EA) coupled with an isotope ratio mass spectrometer (Thermo Fisher Scientific Delta V Plus) at the Institute of Earth Surface Dynamics, University of Lausanne (UNIL), following the protocol described in Spangenberg (2016). The $\delta^{13}C_{org}$ values were used to generate a local climate record comparable to composite reference curves rather than $\delta^{13}C_{carb}$ values, which may have been affected by diagenetic and lithologic effects, and because global trends in $\delta^{13}C_{org}$ mimic those of $\delta^{13}C_{carb}$, as previously demonstrated (e.g., Khozyem et al., 2013). Whole-rock organic matter was analyzed using a Rock-Eval 6 (calibrated with IFP 160000 standard) at the Institute of Earth Sciences (UNIL) (Espitalie et al., 1985). The Rock-Eval pyrolysis allowed the hydrogen and oxygen indices (HI, OI), T_{max}, and total organic carbon (TOC) content to be determined. The $\delta^{13}C_{org}$ and Rock-Eval results are provided as Supplemental Material[1].

DEPOSITIONAL SETTINGS AND GEOCHEMISTRY

Bioclast-rich limestone beds (containing benthic foraminifera, oysters, and echinoderms) with a packstone-to-wackestone texture constitute the base of the Morillo Limestone and occur sporadically up section within the Castigaleu Formation (Figs. 2A and 3). These limestone beds record deposition in midramp platform environments (Chanvry et al., 2018). The Castigaleu Formation (Figs. 2 and 3) consists of cross-bedded sandstones interbedded with massive-to-laminated mudstones (Figs. 2A–2F and 3). Sandstone beds have sharp bases and are predominantly massive or trough cross-stratified with single or double mud drapes on the foresets (Figs. 2B and 2C), occasionally displaying wood debris and symmetrical ripples. Bioturbation in sandstones and mudstones is sparse (Figs. 2D–2F). Meter-thick mudstones sporadically accumulated large benthic foraminifera (Fig. 2G). These observations suggest a deltaic environment, where massive-to-laminated mudstones with interbedded sandstone layers point to deeper-water prodelta settings. In contrast, cross-stratified sandstone beds reflect shallower subtidal bar and tide-dominated delta-front deposits (Nijman, 1998; Chanvry et al., 2018). The vertical succession of these depositional environments shows alternating progradation and retrogradation organized in short-term sequences (S in Fig. 3; defined by Chanvry et al., 2018), spanning hundreds of meters, and elementary sequences (E in Fig. 3) defined at a tens-of-meters scale (Figs. 2A, 2H, 2I, and 3). Sequences are defined from coarsening- and fining-upward trends bounded by maximum flooding surfaces.

The $\delta^{13}C_{org}$ values range from –28.7‰ to –19.4‰ and depict several negative CIEs (Fig. 3). TOC contents are relatively low, ranging from 0.02 to 1.49 wt%. Samples with TOC >0.2 wt% have HI, OI, and T_{max} values spanning 0–126.1 mg HC g^{-1} TOC, 21.3–236.1 mg CO_2 g^{-1} TOC, and 401.8–492 °C, respectively (Supplemental Material). These values suggest that the organic matter present in the strata is terrestrially dominated, and the cluster at the transition from thermally immature to mature states (see Supplemental Material) suggests a uniform burial history along the section and limited diagenetic overprint (Espitalie et al., 1985).

The statistical comparison of the $\delta^{13}C_{org}$ with TOC (Pearson correlation coefficient, $r = -0.25$), HI ($r = 0.11$), OI ($r = 0.18$), and T_{max} ($r = -0.09$) values suggests no covariance among the data (Supplemental Material). This absence of correlation indicates that the measured $\delta^{13}C_{org}$ profile is little influenced by potential lithologic/source effects and likely largely reflects changes in the $\delta^{13}C$ composition of the atmosphere (Arens et al., 2000). The $\delta^{13}C_{org}$ trends persist even when considering only data from mudstone samples (Supplemental Material). Matching magnetozones (c23n.2r, c23n.2n, c23n.1r, c23n.1n, c22r; Fig. 3) between Bentham and Burbank (1996) and Westerhold et al. (2020) allow tentative correlation between the measured $\delta^{13}C_{org}$ record and coeval $\delta^{13}C_{carb}$ and $\delta^{18}O_{carb}$ reference records (Fig. 3; Westerhold

[1]Supplemental Material. Two figures and one table providing additional information about the stratigraphic log, including Rock-Eval pyrolysis and carbon isotope data. Please visit https://doi.org/10.1130/GEOL.S.27097435 to access the supplemental material; contact editing@geosociety.org with any questions.

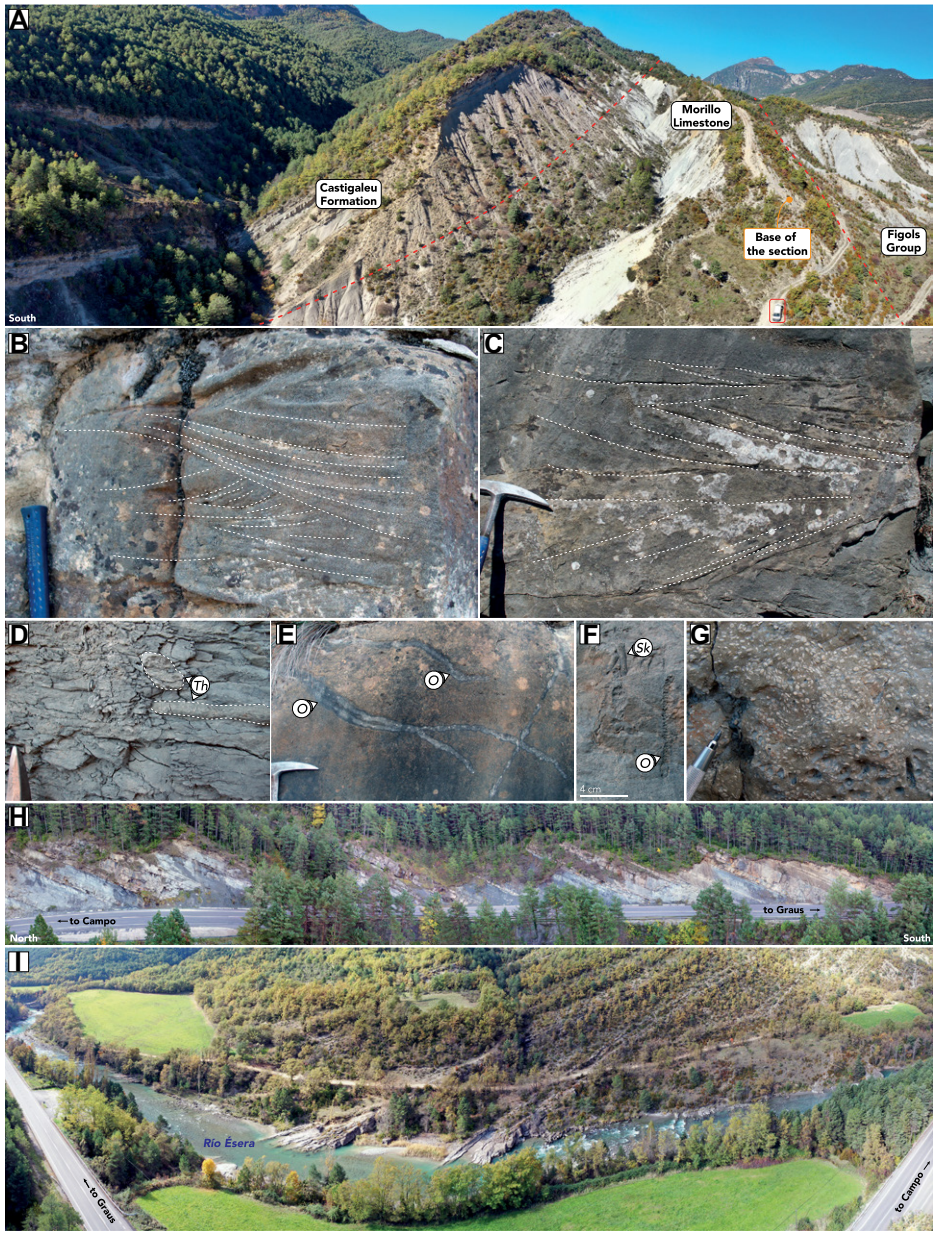

Figure 2. (A) Castigaleu Formation overlying Morillo Limestone. Car for scale. (B) Fine-grained, low-angle trough cross-bedded sandstone. (C) Fine-grained, cross-bedded sandstone exhibiting single and double mud drapes on foresets and symmetrical cross-lamination. (D) *Thalassinoides* (*Th*) traces within massive silty mudstone. (E) Large *Ophiomorpha* (*O*) traces within fine-grained cross-bedded sandstones. (F) *Skolithos* (*Sk*) and *Ophiomorpha* (*O*) traces within massive to laminated medium-grained sandstone. (G) Accumulation of benthic foraminifera, predominantly comprising *Nummulites* and *Alveolina*. (H) Middle part of section illustrating recurrent alternation between cross-stratified sandstones and massive to laminated mudstones. (I) Overview of upper part of studied section. See Supplemental Material for stratigraphic position of figures (text footnote 1).

et al., 2020). This correlation allows us to estimate that the studied interval spans from ca. 52.2 to 50.6 Ma. Hyperthermal events M, N, O, P, Q, and R (Westerhold et al., 2020) occurred during this time interval (Fig. 3).

DISCUSSION AND CONCLUSION

The stacking pattern of the studied interval reveals repetitive retrogradation and progradation trends at both large and small scales (Fig. 3), implying fluctuations in δA and/or δS. Sequences S1–S6 (Fig. 3) are recorded in coeval strata along a depositional dip section that favors a basinwide signal over lateral delta migration (Chanvry et al., 2018). Autogenic variations are expected to be limited due to the confined nature of the Tremp Basin (Chanvry et al., 2018), as well as the tidal influence on the delta fed by multiple rivers, which reduces the likelihood of large-scale avulsions (Plink-Björklund, 2012). The presumed ice-free conditions during the EECO (Westerhold et al., 2020) suggest that eustatic fluctuations were limited and had minimal influence on the stacking pattern. Moreover, at the basin scale, the studied interval has been interpreted to correspond to a long-term transgression driven by increased basin flexure (Chanvry et al., 2018).

A correlation between $\delta^{13}C_{org}$ and the $\delta^{13}C_{carb}$ reference curve was established by matching local and reference magnetozones (Fig. 3). Several negative CIEs in $\delta^{13}C_{org}$, identified by their stratigraphic positions and patterns, systematically correlate to progradation phases of E sequences (Fig. 3), with some coinciding with hyperthermal events (M, N, O, P; Fig. 3), which in turn correspond to the onset or end of most of the progradation S sequences (Fig. 3). Deltas are prone to erosion, reworking, variable sedimentation rate, and bypassing, potentially causing hiatuses or time-dilated intervals in the stratigraphy. These processes could explain the variable positions of negative CIEs in the $\delta^{13}C_{org}$ record in the progradation sequences (S1–S3, S5; Fig. 3) linked to hyperthermal events (M, N, O, P; Fig. 3) and justify discrepancies between $\delta^{13}C_{org}$ and $\delta^{13}C_{carb}$ without inferring an allogenic influence (Fig. 3). Furthermore, the differences in amplitude between the CIEs in the $\delta^{13}C_{org}$ and $\delta^{13}C_{carb}$ records may be attributed to local climate effects related to precipitation patterns distorting the terrestrially dominated $\delta^{13}C_{org}$ profile (Kohn, 2010). However, the exact origin of these discrepancies between $\delta^{13}C_{org}$ and $\delta^{13}C_{carb}$ falls beyond the scope of this study, and shifts toward negative $\delta^{13}C_{org}$ remain associated with progradation trends (Fig. 3).

The progradation trends correlating with hyperthermal events (M, N, O, P; Fig. 3), together with the limited eustatic sea-level fluctuation (Westerhold et al., 2020), the increased basin flexure, and the evidence for long-term transgressive trends at the basin scale during the studied interval (Chanvry et al., 2018), favor the hypothesis of δS as the trigger for recurrent progradation of the tide-dominated delta into the basin. In addition, studies suggest that hyperthermal events during the EECO, aligned with eccentricity maxima that enhanced seasonal variations and hydrological cycles, may have increased detrital input (e.g., Zhang et al., 2024), supporting the δS hypothesis. Regarding the E sequences (Fig. 3), while autogenic processes cannot be dismissed, their consistent alignment with negative CIEs in $\delta^{13}C_{org}$ suggests that δS via climate variability may also have played a role.

Conceptually, the negative CIEs (Fig. 3), indicative of hyperthermal events during the EECO, were linked to rapid increases in temperature and intensified precipitation that triggered erosion and chemical weathering on land (Zachos et al., 2008), which subsequently increased the siliciclastic flux to the ocean (t_0, t_2; Fig. 4). Negative CIEs occurred during progra-

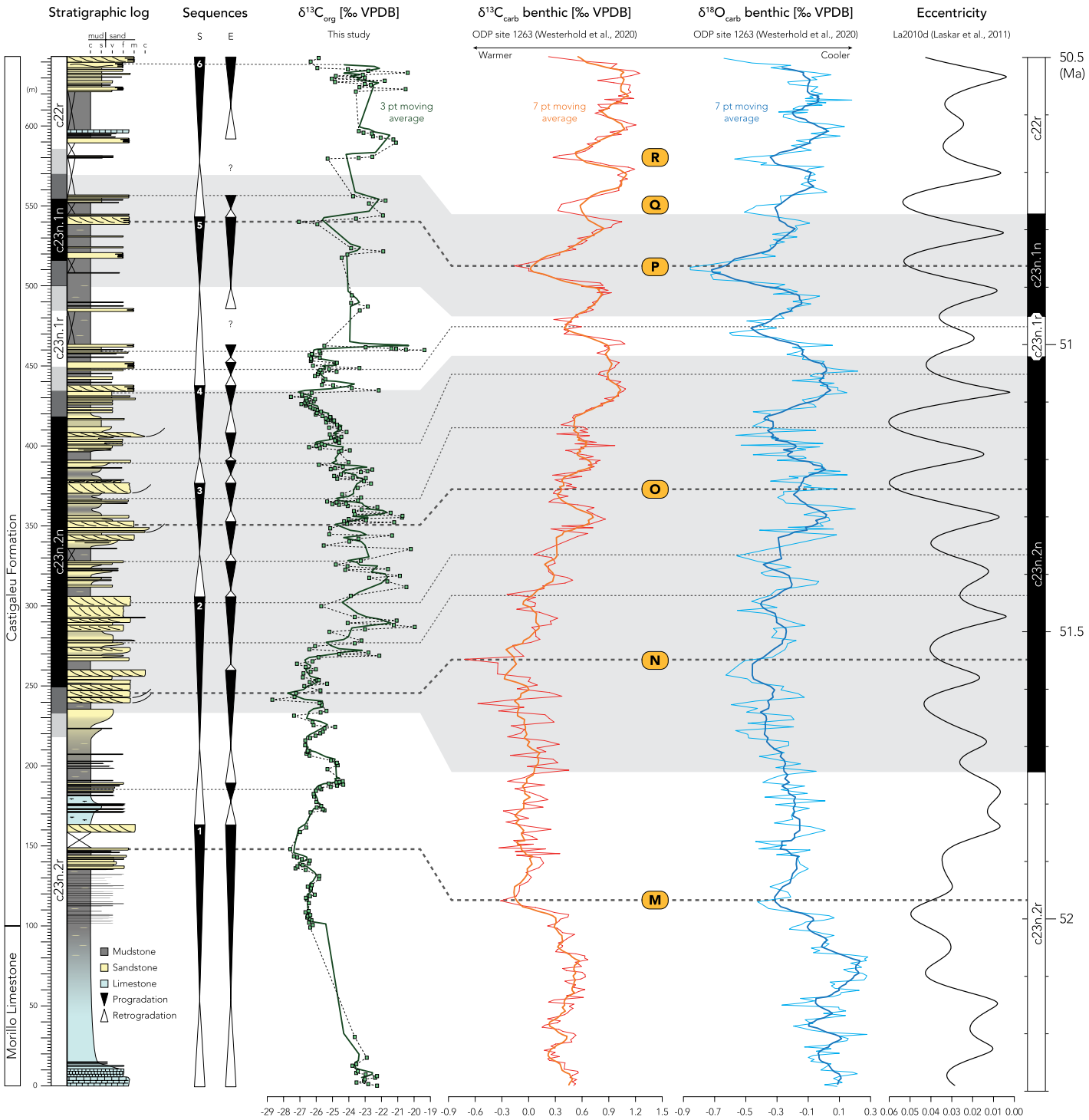

Figure 3. Stratigraphic log of studied section along Río Ésera with corresponding $\delta^{13}C_{org}$ values. Magnetic polarity zones are from Bentham and Burbank (1996). Main depositional sequences are shown (S—short-term sequences; E—elementary sequences). S sequences are from Chanvry et al. (2018). Dashed lines indicate correlation between sequence and measured $\delta^{13}C_{org}$, and some of these correlations have been extended to $\delta^{13}C_{carb}$ and $\delta^{18}O_{carb}$ values (Westerhold et al., 2020) and eccentricity cycles (Laskar et al., 2011). Observed excursions toward more negative $\delta^{13}C$ values are consistently linked with progradation trends. Letters in yellow boxes denote hyperthermal events defined by Westerhold et al. (2020). VPDB—Vienna Peedee belemnite; c—clay; s—silt; v—very-fine sand; f—fine sand; m—medium sand; c—coarse sand.

dation and suggest that $\delta A < \delta S$ (Fig. 4). Conversely, relatively cooler intervals recorded by positive CIEs would have inhibited the hydrological cycle in the hinterland, decreasing siliciclastic sediment flux into the basin and potentially promoting upstream aggradation. Coupled with continuous subsidence, the $\delta A > \delta S$ (t_1; Fig. 4) conditions led to the retrogradation of the system, which promoted the accumulation of carbonate-rich levels during retrogradation, reflecting reciprocal sedimentation (Wilson, 1967). The record of recurrent progradation phases during warming events aligns with numerical simulation results indicating that sedimentary basins are more sensitive to short-term climate-induced δS rather than long-term tectonically induced δS (Simpson and Castelltort, 2012). Furthermore, the relatively short transfer

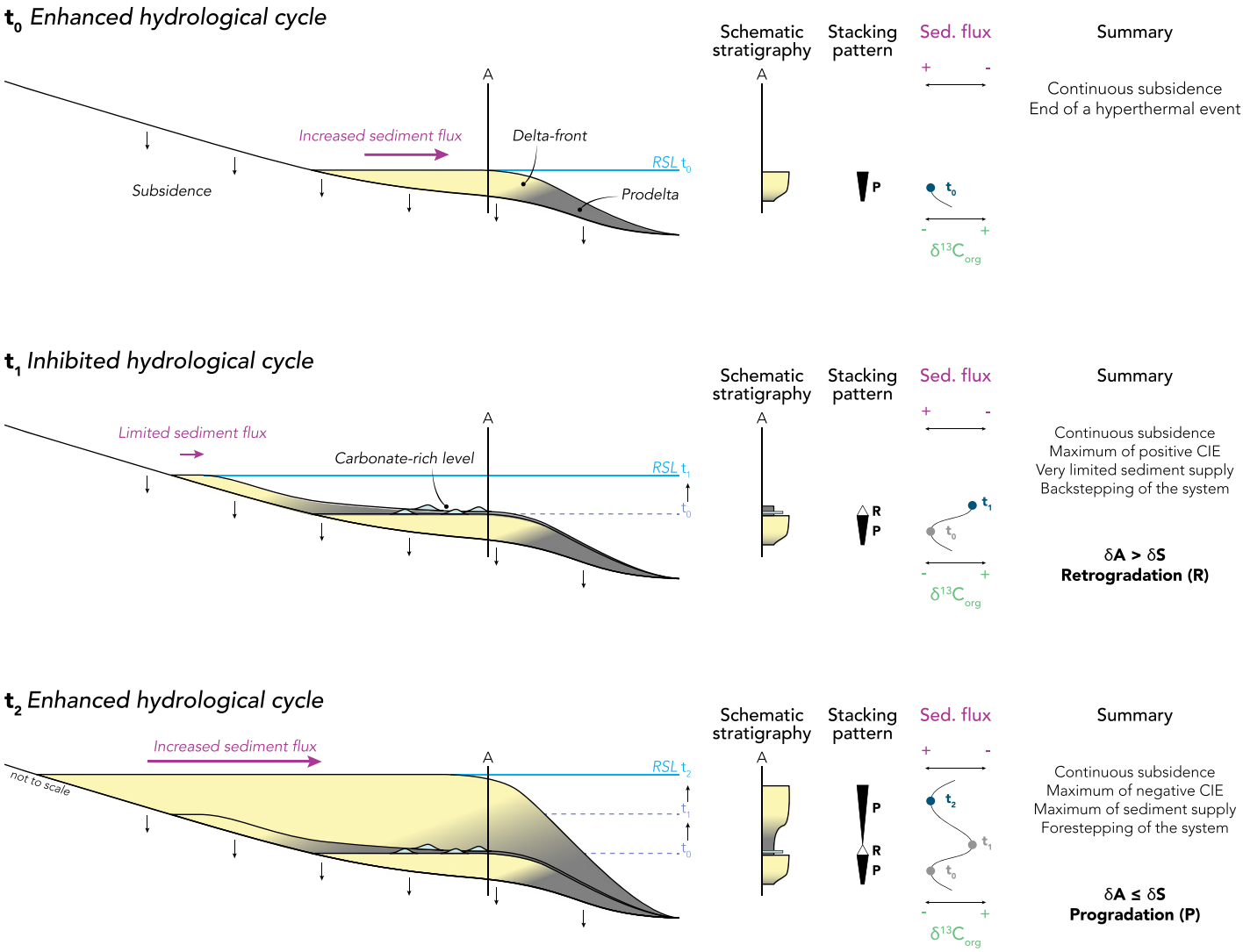

Figure 4. Conceptual model of supply-driven delta sequences during the early Eocene in the Tremp Basin. Studied section is marked as A. Stage t_0 starts at end of a hyperthermal event. Stage t_1 is phase of restricted sediment influx into basin, manifested by retrogradation of delta, favoring accumulation of carbonate layers in basin. Siliciclastic sediment flux decreased as consequence of inhibited hydrological cycle. Stage t_2 corresponds to period characterized by hyperthermal event that amplifies supply to basin, resulting in progradation of delta. RSL—relative sea level; δA—accommodation; δS—sediment supply; CIE—carbon isotope excursion.

zone in the Tremp Basin (Fig. 1C) favors direct source-to-sink transfer of sediment over a short period of time, promoting the preservation of high-frequency climate signals (Castelltort and Van Den Driessche, 2003; Tofelde et al., 2021; Vaucher et al., 2021).

In conclusion, our study underscores δS as a major control on delta sequences during the early Eocene in the Tremp Basin. This study contributes to broader understanding of the profound impact of climate change on shallow-marine systems, reinforcing the importance of considering sediment supply variations in the interpretation of depositional sequences.

ACKNOWLEDGMENTS

This research was funded through a Swiss National Science Foundation grant to R. Vaucher (P5R5PN_202846). Guillaume Suan and Tiffany Monnier are thanked for feedback on the manuscript and help in the laboratory, respectively. Peter Burgess, Tor Sømme, and Allard Martinius are warmly thanked for their constructive reviews.

REFERENCES CITED

Arens, N.C., Jahren, A.H., and Amundson, R., 2000, Can C3 plants faithfully record the carbon isotopic composition of atmospheric carbon dioxide?: Paleobiology, v. 26, p. 137–164, https://doi.org/10.1666/0094-8373(2000)026<0137:CCPFRT>2.0.CO;2.

Bentham, P., and Burbank, D.W., 1996, Chronology of Eocene foreland basin evolution along the western oblique margin of the south-central Pyrenees, *in* Dabrio, C.J., and Friend, P.F., eds., Tertiary Basins of Spain: The Stratigraphic Record of Crustal Kinematics: Cambridge, UK, Cambridge University Press, p. 144–152, https://doi.org/10.1017/CBO9780511524851.022.

Burgess, P.M., 2016, The future of the sequence stratigraphy paradigm: Dealing with a variable third dimension: Geology, v. 44, p. 335–336, https://doi.org/10.1130/focus042016.1.

Burgess, P.M., and Prince, G.D., 2015, Non-unique stratal geometries: Implications for sequence stratigraphic interpretations: Basin Research, v. 27, p. 351–365, https://doi.org/10.1111/bre.12082.

Castelltort, S., and Van Den Driessche, J., 2003, How plausible are high-frequency sediment supply–driven cycles in the stratigraphic record?: Sedimentary Geology, v. 157, p. 3–13, https://doi.org/10.1016/S0037-0738(03)00066-6.

Castelltort, S., Honegger, L., Adatte, T., Clark, J.D., Puigdefàbregas, C., Spangenberg, J.E., Dykstra, M.L., and Fildani, A., 2017, Detecting eustatic and tectonic signals with carbon isotopes in deep-marine strata, Eocene Ainsa Basin, Spanish Pyrenees: Geology, v. 45, p. 707–710, https://doi.org/10.1130/G39068.1.

Catuneanu, O., Abreu, V., Bhattacharya, J.P., Blum, M.D., Dalrymple, R.W., Eriksson, P.G., Fielding, C.R., Fisher, W.L., Galloway, W.E., Gibling, M.R., Giles, K.A., Holbrook, J.M., Jordan, R., Kendall, C.G.S.C., Macurda, B., Martinsen, O.J., Miall, A.D., Neal, J.E., Nummedal, D., Pomar, L., Posamentier, H.W., Pratt, B.R., Sarg, J.F., Shanley, K.W., Steel, R.J., Strasser, A., Tucker, M.E., and Winker, C., 2009, Towards the standardization of sequence stratigraphy: Earth-Science Re-

views, v. 92, p. 1–33, https://doi.org/10.1016/j.earscirev.2008.10.003.
Chanvry, E., Deschamps, R., Joseph, P., Puigdefàbregas, C., Poyatos-Moré, M., Serra-Kiel, J., Garcia, D., and Teinturier, S., 2018, The influence of intrabasinal tectonics in the stratigraphic evolution of piggyback basin fills: Towards a model from the Tremp-Graus-Ainsa Basin (South-Pyrenean zone, Spain): Sedimentary Geology, v. 377, p. 34–62, https://doi.org/10.1016/j.sedgeo.2018.09.007.
Chen, C., Guerit, L., Foreman, B.Z., Hassenruck-Gudipati, H.J., Adatte, T., Honegger, L., Perret, M., Sluijs, A., and Castelltort, S., 2018, Estimating regional flood discharge during Palaeocene–Eocene global warming: Scientific Reports, v. 8, 13391, https://doi.org/10.1038/s41598-018-31076-3.
Espitalie, J., Deroo, G., and Marquis, F., 1985, La pyrolyse Rock-Eval et ses applications. Première partie: Revue de l'Institut Français du Pétrole, v. 40, p. 563–579, https://doi.org/10.2516/ogst:1985035.
Ford, M., Masini, E., Vergés, J., Pik, R., Ternois, S., Léger, J., Dielforder, A., Frasca, G., Grool, A., Vinciguerra, C., Bernard, T., Angrand, P., Crémades, A., Manatschal, G., Chevrot, S., Jolivet, L., Mouthereau, F.r., Thinon, I., Calassou, S., Tavani, S., Teixell, A., Pedreira, D., and Calassou, S., 2022, Evolution of a low convergence collisional orogen: A review of Pyrenean orogenesis: Bulletin de la Société Géologique de France, v. 193, https://doi.org/10.1051/bsgf/2022018.
Foreman, B.Z., Heller, P.L., and Clementz, M.T., 2012, Fluvial response to abrupt global warming at the Palaeocene/Eocene boundary: Nature, v. 491, p. 92–95, https://doi.org/10.1038/nature11513.
Jervey, M.T., 1988, Quantitative geological modeling of siliciclastic rock sequences and their seismic expression, *in* Wilgus, C.K., et al., eds., Sea-Level Changes: An Integrated Approach: Society for Sedimentary Geology (SEPM) Special Publication 42, p. 47–69, https://doi.org/10.2110/pec.88.01.0047.
Khozyem, H., Adatte, T., Spangenberg, J.E., Tantawy, A.A., and Keller, G., 2013, Palaeoenvironmental and climatic changes during the Palaeocene-Eocene thermal maximum (PETM) at the Wadi Nukhul section, Sinai, Egypt: Journal of the Geological Society, v. 170, p. 341–352, https://doi.org/10.1144/jgs2012-046.
Kohn, M.J., 2010, Carbon isotope compositions of terrestrial C3 plants as indicators of (paleo)ecology and (paleo)climate: Proceedings of the National Academy of Sciences of the United States of America, v. 107, p. 19,691–19,695, https://doi.org/10.1073/pnas.1004933107.
Laskar, J., Fienga, A., Gastineau, M., and Manche, H., 2011, La2010: A new orbital solution for the long-term motion of the Earth: Astronomy & Astrophysics, v. 532, p. A89, https://doi.org/10.1051/0004-6361/201116836.
Muñoz, J.A., 1992, Evolution of a continental collision belt: ECORS-Pyrenees crustal balanced cross-section, *in* McClay, K.R., ed., Thrust Tectonics: Dordrecht, Netherlands, Springer, p. 235–246, https://doi.org/10.1007/978-94-011-3066-0_21.
Muñoz, J.A., Beamud, E., Fernández, O., Arbués, P., Dinarès-Turell, J., and Poblet, J., 2013, The Ainsa fold and thrust oblique zone of the central Pyrenees: Kinematics of a curved contractional system from paleomagnetic and structural data: Tectonics, v. 32, p. 1142–1175, https://doi.org/10.1002/tect.20070.
Muto, T., and Steel, R.J., 1997, Principles of regression and transgression: The nature of the interplay between accommodation and sediment supply: Journal of Sedimentary Research, v. 67, p. 994–1000, https://doi.org/10.1306/D42686A8-2B26-11D7-8648000102C1865D.
Nijman, W., 1998, Cyclicity and basin axis shift in a piggyback basin: Towards modelling of the Eocene Tremp-Ager Basin, south Pyrenees, Spain, *in* Mascle, A., et al., eds., Cenozoic Foreland Basins of Western Europe: Geological Society, London, Special Publication 134, p. 135–162, https://doi.org/10.1144/GSL.SP.1998.134.01.07.
Peris Cabré, S., Valero, L., Spangenberg, J.E., Vinyoles, A., Verité, J., Adatte, T., Tremblin, M., Watkins, S., Sharma, N., Garcés, M., Puigdefàbregas, C., and Castelltort, S., 2023, Fluvio-deltaic record of increased sediment transport during the middle Eocene climatic optimum (MECO), southern Pyrenees, Spain: Climate of the Past, v. 19, p. 533–554, https://doi.org/10.5194/cp-19-533-2023.
Plink-Björklund, P., 2012, Effects of tides on deltaic deposition: Causes and responses: Sedimentary Geology, v. 279, p. 107–133, https://doi.org/10.1016/j.sedgeo.2011.07.006.
Prieur, M., Whittaker, A.C., Nuriel, P., Jaimes-Gutierrez, R., Garzanti, E., Roigé, M., Sømme, T.O., Schlunegger, F., and Castelltort, S., 2024, Fingerprinting enhanced floodplain reworking during the Paleocene-Eocene thermal maximum in the southern Pyrenees (Spain): Implications for channel dynamics and carbon burial: Geology, v. 52, p. 651–655, https://doi.org/10.1130/G52180.1.
Puigdefàbregas, C., and Souquet, P., 1986, Tecto-sedimentary cycles and depositional sequences of the Mesozoic and Tertiary from the Pyrenees: Tectonophysics, v. 129, p. 173–203, https://doi.org/10.1016/0040-1951(86)90251-9.
Schlager, W., 1993, Accommodation and supply—A dual control on stratigraphic sequences: Sedimentary Geology, v. 86, p. 111–136, https://doi.org/10.1016/0037-0738(93)90136-S.
Simpson, G., and Castelltort, S., 2012, Model shows that rivers transmit high-frequency climate cycles to the sedimentary record: Geology, v. 40, p. 1131–1134, https://doi.org/10.1130/G33451.1.
Spangenberg, J.E., 2016, Bulk C, H, O, and fatty acid C stable isotope analyses for purity assessment of vegetable oils from the Southern and Northern Hemispheres: Rapid Communications in Mass Spectrometry, v. 30, p. 2447–2461, https://doi.org/10.1002/rcm.7734.
Tofelde, S., Bernhardt, A., Guerit, L., and Romans, B.W., 2021, Times associated with source-to-sink propagation of environmental signals during landscape transience: Frontiers of Earth Science, v. 9, https://doi.org/10.3389/feart.2021.628315.
Vaucher, R., Dashtgard, S.E., Horng, C.-S., Zeeden, C., Dillinger, A., Pan, Y.-Y., Setiaji, R.A., Chi, W.-R., and Löwemark, L., 2021, Insolation-paced sea level and sediment flux during the early Pleistocene in Southeast Asia: Scientific Reports, v. 11, 16707, https://doi.org/10.1038/s41598-021-96372-x.
Vimpere, L., Spangenberg, J.E., Roige, M., Adatte, T., De Kaenel, E., Fildani, A., Clark, J., Sahoo, S., Bowman, A., Sternai, P., and Castelltort, S., 2023, Carbon isotope and biostratigraphic evidence for an expanded Paleocene-Eocene thermal maximum sedimentary record in the deep Gulf of Mexico: Geology, v. 51, p. 334–339, https://doi.org/10.1130/G50641.1.
Westerhold, T., Marwan, N., Drury, A.J., Liebrand, D., Agnini, C., Anagnostou, E., Barnet, J.S.K., Bohaty, S.M., De Vleeschouwer, D., Florindo, F., Frederichs, T., Hodell, D.A., Holbourn, A.E., Kroon, D., Lauretano, V., Littler, K., Lourens, L.J., Lyle, M., Pälike, H., Röhl, U., Tian, J., Wilkens, R.H., Wilson, P.A., and Zachos, J.C., 2020, An astronomically dated record of Earth's climate and its predictability over the last 66 million years: Science, v. 369, p. 1383–1387, https://doi.org/10.1126/science.aba6853.
Wilson, J.L., 1967, Cyclic and reciprocal sedimentation in Virgilian strata of southern New Mexico: Geological Society of America Bulletin, v. 78, p. 805–818, https://doi.org/10.1130/0016-7606(1967)78[805:CARSIV]2.0.CO;2.
Zachos, J.C., Dickens, G.R., and Zeebe, R.E., 2008, An early Cenozoic perspective on greenhouse warming and carbon-cycle dynamics: Nature, v. 451, p. 279–283, https://doi.org/10.1038/nature06588; erratum available at https://doi.org/10.5194/cp-14-1515-2018.
Zhang, J., Burgess, P.M., Granjeon, D., and Steel, R., 2019, Can sediment supply variations create sequences? Insights from stratigraphic forward modelling: Basin Research, v. 31, p. 274–289, https://doi.org/10.1111/bre.12320.
Zhang, R., Huang, C., Kemp, D.B., Zhang, Z., Wang, Z., Zhang, X., Zhao, D., Jin, S., and Zhang, R., 2024, Eccentricity forcing of the hydrological cycle in East Asia during the early Eocene climatic optimum (EECO): Journal of Geophysical Research: Atmospheres, v. 129, https://doi.org/10.1029/2023JD040314.

Printed in the USA